fakultät für mathematik

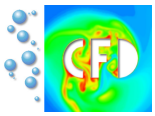

Feat-Flow Lab Report SS2011

Numerical study of flow across multiple obstacles in a uniform stream of infinite extent for low Reynolds numbers and various angles of attack of the upstream velocity.

supervised by

Dr. Mudassar Razzaq

Dr. Ludmila Rivkind

Technische Universität Dortmund

Fakultät für Mathematik, Lehrstuhl LSIII

Vogelpothsweg 87, 44227 Dortmund

technische universität dortmund

Project

Numerical study of flow across multiple obstacles in a uniform stream of infinite extent for low Reynolds numbers and various angles of attack of the upstream velocity.

Aim

- Examine a two-dimensional low Reynolds number flow over obstacles immersed in a stream of infinite extent.
- The magnitude of the uniform upstream velocity $|\mathbf{u}(U_x, U_y)|_\infty = U_\infty = 1$.
- Study the problem for Reynolds number in the range $1 \leq Re \leq 100$ and the angle of attack of the upstream velocity at $\alpha = -5°; 0°; 5°$.
- Analyse the resulting drag and lift forces acting on obstacles with respect to the angle of attack of the upstream velocity and the Reynolds number.
- Determine the influence of one obstacle onto the resulting drag and lift coefficients of other obstacles.

Aerodynamic problem

We consider the two-dimensional, steady , incompressible, viscous fluid at low Reynolds number with an uniform velocity U_∞ around the circular and elliptical cylinders in unbounded domain. The governing Navier-Stokes equations in terms of dimensional primary variables for the laminar fluid flow are:

$$-\nu \bigtriangledown u + u \cdot \bigtriangledown u + \bigtriangledown p = 0, \bigtriangledown . u = 0 \quad in \quad \Omega$$

with prescribed boundary values on the boundary $\partial\Omega$.
Here, $u(U_x, U_y)$ is a velocity, U_x, U_y are the x and y-components of the velocity, $\rho = 1$ is the density, ν is the kinematic viscosity of the fluid. As common in the mathematical literature (see [**?**]), we consider the viscosity parameter $1/\nu$ as the Reynolds number $Re = UL/\nu$ assuming $L = U = 1$, where L is a characteristic length scale of the flow, U is a characteristic velocity scale of the flow.
Numerical simulation of the problems in a unbounded flow region requires the computational domain to be truncation. According to the results reported in the literature the size of the bounded computational domain has to be enough large to provide accurate results for low Reynolds numbers.
The boundary conditions on $\partial\Omega$ are prescribed as follows:
On the surface of obstacles (Dirichlet boundary conditions):
$u = 0$ is the standard no-slip condition.

Upstream entrance:
$U_x = \cos\alpha, U_y = \sin\alpha$, where α is the angle of attack of the upstream velocity.
Downstream outflow:
$\nu\frac{\partial u}{\partial n} - pn = 0$, is the so-called 'do-nothing' boundary conditions.

Numerical methodology

- **Problem Solver**
  The numerical study is carried out using the code cc2d which is the part of the FEATFLOW1.1 software. The FEATFLOW package is the solver package for viscous, incompressible fluid flow in 2D and 3D for both stationary and non stationary problems. The Navier-Stokes equations are approximated using a finite element method for the spatial discretization with nonconforming quadrilateral finite elements.
  The code cc2d is a direct, fully coupled approach for solving the discrete version of the incompressible Navier-Stokes equations for 2D flows at low and intermediate Reynolds numbers.
  The nonlinear algebraic systems are exploited by iterative solution methods. The nonlinear problems are treated by the adaptive fixed point defect correction method. The linear subproblems are solved by a multigrid method. The Multigrid method uses hierarchy of grids. The code cc2d divides each quadrilateral of the coarse mesh into four quadrilaterals to form the next fine mesh. The Multigrid algorithm visits all coarser grids in order given by multigrid cyrcle (in our simulation - type F). At the end of this process we have the solution on the finest mesh.
  The Samarskij weighted upwind scheme is used for stabilization of convective terms.

- **Preprocessing**
  The coarse grid are defined by two files which are generated using preprocessing tool DeViSoRgrid.

- **Postprocessing**
  The process of visualisation is based on tool The General Mesh Viewer.
  Graphics were created using the Gnuplot program.

Contents

1 Task I

Title: Numerical study of flow across an ellipse and a circle placed in a uniform stream of infinite extent. The x-component of the upstream velocity $U_x \leq 0$.

Submitted by:

- Rajesh, Koduri
- Mohammed Shahfir, Kajah Najmudeen

Aim

- Examine a two-dimensional low Reynolds number flow around the ellipse and the circle immersed in a stream of infinite extent (see Fig.1.1).
- The x-component of the upstream velocity $U_x \leq 0$.
- The magnitude of the uniform upstream velocity $|\mathbf{u}(U_x, U_y)|_\infty = U_\infty = 1$.
- Study the problem for Reynolds number in the range $1 \leq Re \leq 100$ and the angle of attack of the upstream velocity at $\alpha = -5°; 0°; 5°$.
- Analyse the resulting drag and lift forces acting on obstacles with respect to the angle of attack of the upstream velocity and the Reynolds number.
- Determine the influence of the circle onto the resulting drag and lift coefficients of the ellipse.

1.1 Computational domain

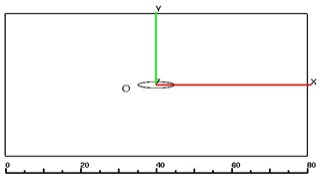

Fig.1.1 Computational Domain

- **The exterior geometry of the rectangle:**
  $h = 40.0,\ l = 80.0$ - height and width of the bounding box.
  $C(0.0, 0.0)$ is the position of the center of the rectangle.
  $(-40.0, -20.0)$ is the point of the left lower corner of the box.
  $(40.0, 20.0)$ is the point of the right upper corner of the box.

- **Position of the ellipse (boundary 2):**

  $h1 = 2.0,\ l1 = 10.0$ - height and width of the ellipse.

  $C(0.0, 0.0)$ is the position of the center of the ellipse.

  $E = 5$ is the aspect ratio of the ellipse ($E = l1/h1$).

- **Position of the circle (boundary 3):**

  $R = 0.5$ is the radius of the circle with its center at $C(-8.0, -1.0)$.

1.2 Implementation of Boundary conditions

- **The case of $\alpha = 0^0$**

  Upstream entrance (the Dirichlet boundary conditions):

  $U_x = -1.0, U_y = 0.0$ on the line: $x = 40.0$; $-20.0 \leq y \leq 20.0$.

  Downstream exit (Do nothing's" boundary conditions):

  on the line: $-40.0 \leq x \leq 40.0$; $y = 20.0$.

  on the line: $-40.0 \leq x \leq 40.0$; $y = -20.0$.

  on the line $x = -40.0$; $-20.0 \leq y \leq 20.0$.

- **In the case of $\alpha = 5^\circ$**

  Upstream entrance:the Dirichlet boundary condition

  $U_x = \cos(\alpha), U_y = \sin(\alpha)$ on the line: $x = 40.0$; $-20.0 \leq y \leq 20.0$.

  $U_x = \cos(\alpha), U_y = \sin(\alpha)$ on the line: $-40.0 \leq x \leq 40$; $y = -20.0$.

  Downstream exit: "Do nothing's" boundary conditions

  on the line: $-40.0 \leq x \leq 40.0$; $y = 20.0$.

  on the line: $x = -40.0$; $-20.0 \leq y \leq 20.0$.

- **In the case of $\alpha = -5^\circ$**

  Upstream entrance:the Dirichlet boundary condition

  $U_x = \cos(\alpha), U_y = \sin(\alpha)$ on the line: $x = 40.0$; $-20 \leq y \leq 20$.

  $U_x = \cos(\alpha), U_y = \sin(\alpha)$ on the line: $-40.0 \leq x \leq 40.0$; $y = 20.0$.

  Downstream exit: "Do nothing's" boundary conditions

  on the line:$-40.0 \leq x \leq 40.0$; $y = -20.0$.

  on the line: $x = -40.0$; $-20.0 \leq y \leq 20.0$.

1.3 Spatial Discretization, Mesh refinement and Computational requirements in the code cc2d

We perform series of calculations on different solution levels: 3 - 7.

Table 1.1 presents the progression of grid sizes through seven levels and the typical computational

requirement.

Information about mesh refinement, memory capacity and computational time (Total Time) is available in the protocol file.

Table 1.1 Mesh refinement and computational requirements.

Level	NEL	NMT	d.o.f	IWMAX	Total Time
Lev 1: coarse mesh	102	221	544	0.064MB	0.06sec
Lev 5 : mesh	26.112	52.496	131.104	19.67MB	30.51sec
Lev 7 : finest mesh	417.792	836.672	2.091.136	313.82MB	1632.07sec

NEL is the total number of cells associated with pressure unknowns.

NMT is the total number of midpoints of edges associated with x- and y- components velocity unknowns.

Degrees of freedom d.o.f.'s is expressed by NEL+2*NMT.

IWMAX is the amount of memory in MB.

The coarse mesh which covers the whole domain is presented in Figure 1.2, the part of the mesh around the obstacles on level 2 is present in Figure 1.3(a)and the part of the mesh around the obstacles on level 3 is present in Figure 1.3(b).

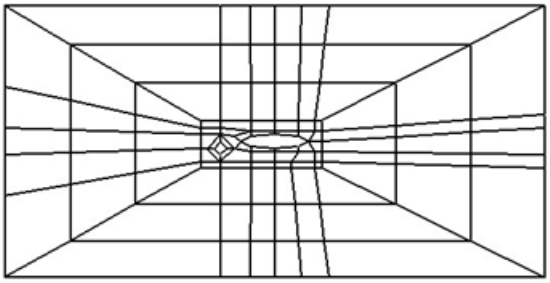

Fig. 1.2 The coarse mesh (level 1)

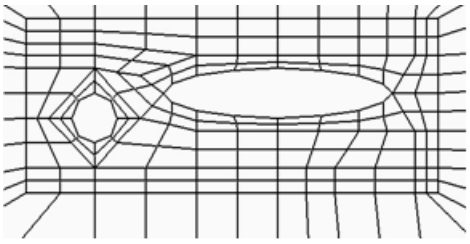

Fig.1.3(a) Mesh on level 2

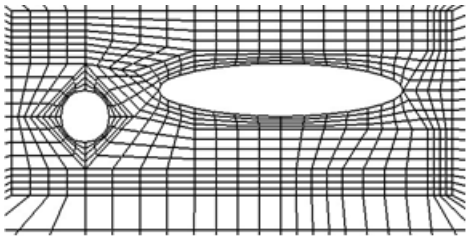

Fig.1.3(b) Mesh on level 3.

1.4 Investigation of the accuracy of the solution:

The mesh refinement is needed to improve solution accuracy across the whole domain. We can control the relative accuracy of a solution to compare solutions on levels 3 - 7 with a solution on a finest mesh (level 7). The table 1.2 shows the change in drag coefficient C_{drag} depending on the mesh refinement.

The calculations were made for $Re = 10, \alpha = -5°$. Reference value C_{ref} is the drag coefficient of the ellipse on the finest mesh (level 7).

Table 1.2. The behaviour of drag coefficient C_{drag} of the ellipse according to computational levels for $Re = 10, \alpha = -5°$

Level	3	4	5	6	7
C_{drag}	2.1455	2.0841	2.0683	2.0671	2.0652
$(C_{drag}$-$C_{ref})/C_{ref}$	3.88%	0.92%	0.15 %	0.02%	0.0%

1.5 Results and Conclusions

- The 2D steady incompressible, viscous flow past the circle and ellipse was investigated numerically.
- The magnitude of the uniform upstream velocity $|\mathbf{u}(U_x, U_y)|_\infty = 1$.
- The x-component of the upstream velocity $U_x \geq 0$.
- The problem has been solved over a range of Reynolds numbers $1 \leq Re \leq 100$ and the angle of attack of the upstream velocity $\alpha = -5°; 0°; 5°$.
- Drag force:
  a. Drag force decreases as Reynolds number increases (see Fig 1.4a).
  b. Drag force very slightly increases as angle of attack α increases (see Fig 1.4(a),1.5).
- Lift Force:
  a. The lift coefficient varies significantly with angle of the attack (see Fig. 1.4(b):
  b. In the case $\alpha = 0$ the lift coefficient converges very rapidly to 0 as Reynolds number increases.
  c. In the case $\alpha = 5°$ the lift coefficient decreases as Reynolds number increases.
  d. In the case $\alpha = -5°$ the lift coefficient increases as Reynolds number increases.
- The effect of the interaction between obstacles were examined (see Fig. 1.6 - 1.7). It can be seen that the value of the drag force acting on an isolated ellipse is larger than those obtained by the corresponding simulation of flow past two obstacles.
- Flow patterns were investigated.
- Fig. 1.8 - 1.11 show velocity magnitude contours. It can be infer that for Re=10 velocity drops around obstacles and when Reynolds number increases velocity around obstacles also increases and streamlines becomes sharper.
- The phenomena of flow recirculation and separation in the rear of the both cylinders are observed for $Re \geq 20$. The usual formation of clockwise and counter-clockwise vortex pairs take place. The length of this vortex formation increases with Re.

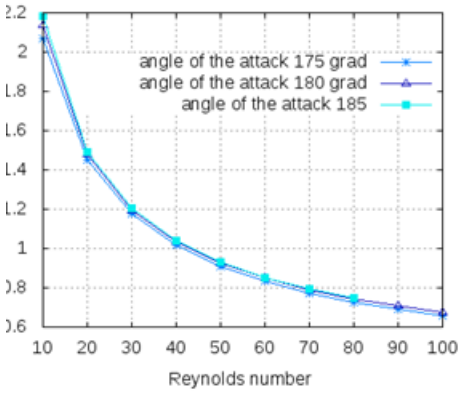

(a) Drag coefficient

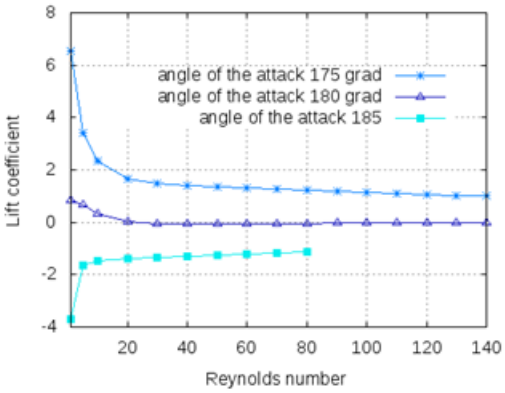

(b) Lift coefficient

Fig.1.4 Variation of drag (a) and lift (b) coefficients of ellipse with the different Reynolds numbers and the angle of attacks

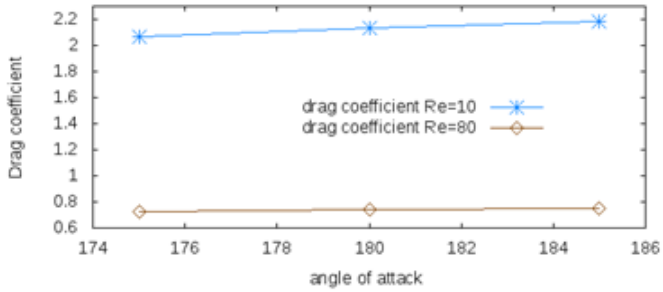

Fig.1.5 Variation of drag coefficient of the ellipse with the angle of attack $-5^\circ \leq \alpha \leq 5^\circ$ and $Re = 10, 80$.

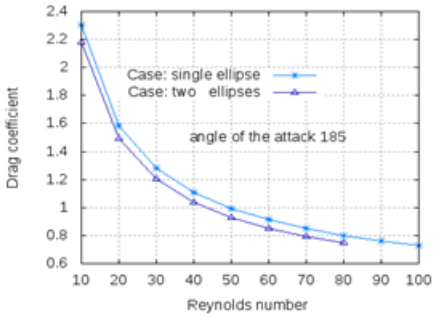

(a) Drag coefficient $\alpha = -5^\circ$

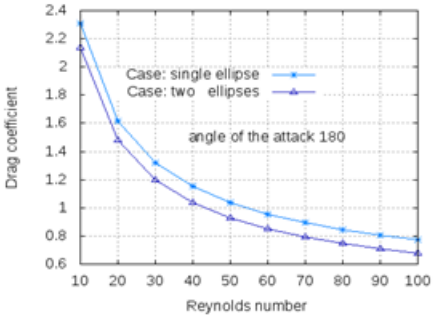

(b) Drag coefficient a$\alpha = 0^\circ$

Fig.1.6 Drag coefficient of an isolated ellipse and Drag coefficient of an ellipse obtained by corresponding simulation of flow past two obstacles at different Re and $\alpha = -5^\circ(a); \quad \alpha = -0^\circ(b)$

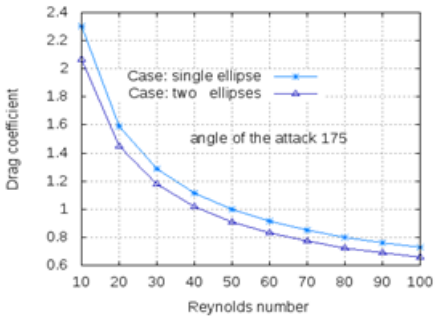

Fig.1.7 Drag coefficient of an isolated ellipse and Drag coefficient of an ellipse obtained by corresponding simulation of flow past two obstacles at different Re and $\alpha = 5^\circ$

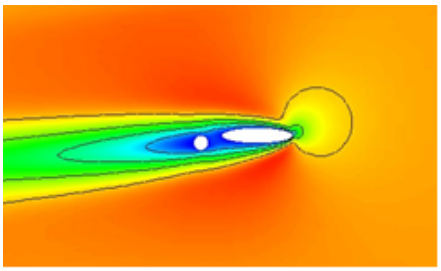

a. $Re = 10$ **and** $\alpha = -5°$

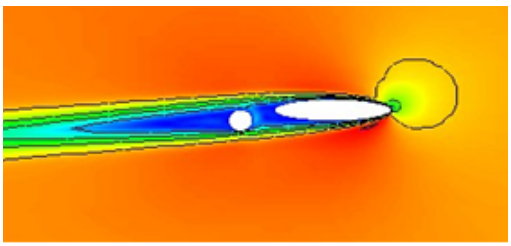

b. $Re = 80$ **and** $\alpha = -5°$

Fig.1.8 Velocity magnitude plot

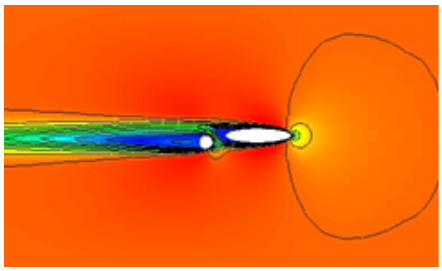

a. $Re = 10$ **and** $\alpha = 0°$

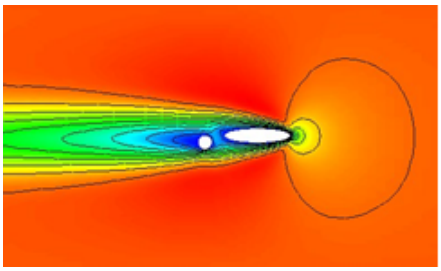

b. $Re = 80$ **and** $\alpha = 0°$

Fig.1.9 Velocity magnitude plot

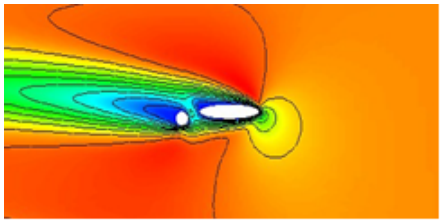

a. $Re = 10$ **and** $\alpha = 5°$

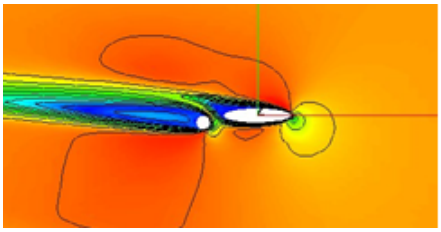

b. $Re = 80$ **and** $\alpha = 5°$

Fig.1.10 Velocity magnitude plot

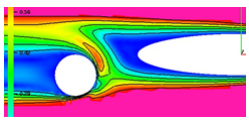

a. $\alpha = 0°$

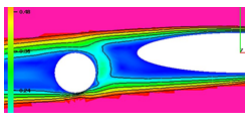

b. $\alpha = 5°$

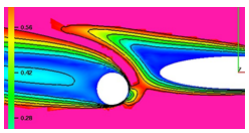

(c) $\alpha = -5°$

Fig.1.11 Velocity magnitude plot around the ellipse at $Re = 80$

2 Task II

Title: Numerical study of flow across an ellipse and a circle placed in a uniform stream of infinite extent. The x-component of the upstream velocity $U_x \geq 0$. **Submitted by:**

- Kushal Patel
- Rajesh Rajendran
- Sandesh Shete

Aim

- Examine a two-dimensional low Reynolds number flow around the ellipse and the circle immersed in a stream of infinite extent (see Fig.2.1).
- The x-component of the upstream velocity $U_x \geq 0$.
- The magnitude of the uniform upstream velocity $|\mathbf{u}(U_x, U_y)|_\infty = U_\infty = 1$.
- Study the problem for Reynolds number in the range $1 \leq Re \leq 100$ and the angle of attack of the upstream velocity at $\alpha = -5°; 0°; 5°$.
- Analyse the resulting drag and lift forces acting on obstacles with respect to the angle of attack of the upstream velocity and the Reynolds number.
- Determine the influence of the circle onto the resulting drag and lift coefficients of the ellipse.

2.1 Computational domain

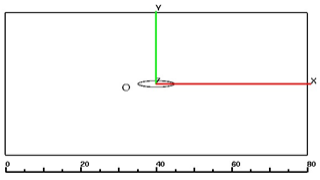

Fig.2.1 Computational Domain

- **The exterior geometry of the rectangle:**
  $h = 40.0,\ l = 80.0$ - height and width of the bounding box.
  $C(0.0, 0.0)$ is the position of the center of the rectangle.
  $(-40.0, -20.0)$ is the point of the left lower corner of the box.
  $(40.0, 20.0)$ is the point of the right upper corner of the box.

- **Position of the ellipse (boundary 2):**

  $h1 = 2.0,\ l1 = 10.0$ - height and width of the ellipse.

  $C(0.0, 0.0)$ is the position of the center of the ellipse.

  $E = 5$ is the aspect ratio of the ellipse ($E = l1/h1$).

- **Position of the circle (boundary 3):**

  $R = 0.5$ is the radius of the circle with its center at $C(-8.0, -1.0)$.

2.2 Implementation of Boundary conditions

- **Case** $\alpha = 0^0$

  Upstream entrance (the Dirichlet boundary conditions):

  $U_x = 1.0, U_y = 0.0$ on the line: $x = -40.0$; $-20.0 \leq y \leq 20.0$.

  Downstream exit (Do nothing's boundary conditions):

  on the line: $-40.0 \leq x \leq 40.0$; $y = 20.0$.

  on the line: $-40.0 \leq x \leq 40.0$; $y = -20.0$.

  on the line $x = 40.0$; $-20.0 \leq y \leq 20.0$.

- **Case** $\alpha = -5^\circ$

  Upstream entrance (the Dirichlet boundary condition):

  $U_x = \cos(\alpha), U_y = \sin(\alpha)$ on the line: $x = -40.0$; $-20.0 \leq y \leq 20.0$.

  $U_x = \cos(\alpha), U_y = \sin(\alpha)$ on the line: $-40.0 \leq x \leq 40$; $y = 20.0$.

  Downstream exit (Do nothing's" boundary conditions):

  on the line: $-40.0 \leq x \leq 40.0$; $y = -20.0$.

  on the line: $x = 40.0$; $-20.0 \leq y \leq 20.0$.

- **Case** $\alpha = 5^\circ$

  Upstream entrance (the Dirichlet boundary condition) :

  $U_x = \cos(\alpha), U_y = \sin(\alpha)$ on the line: $x = -40.0$; $-20 \leq y \leq 20$.

  $U_x = \cos(\alpha), U_y = \sin(\alpha)$ on the line: $-40.0 \leq x \leq 40.0$; $y = -20.0$.

  Downstream exit (Do nothing's boundary conditions):

  on the line:$-40.0 \leq x \leq 40.0$; $y = 20.0$.

  on the line: $x = 40.0$; $-20.0 \leq y \leq 20.0$.

2.3 Spatial Discretization, Mesh refinement and Computational requirements in the code cc2d

We perform series of calculations on different solution levels: 3,4,5,6,7. Table 2.1 presents the progression of grid sizes through seven levels and the typical computational requirement.

Information about mesh refinement, memory capacity and computational time (Total Time) is available in the protocol file.

Table 2.1. Mesh refinement and computational requirements.

Level	NEL	NMT	d.o.f	IWMAX	Total Time
Lev 1: coarse mesh	102	221	544	0.064MB	0.06sec
Lev 5 : mesh	26.112	52.496	131.104	19.67MB	30.51sec
Lev 7 : finest mesh	417.792	836.672	2.091.136	313.82MB	1632.07sec

NEL is the total number of cells associated with pressure unknowns.
NMT is the total number of midpoints of edges associated with x- and y- components velocity unknowns. Degrees of freedom d.o.f.'s is expressed by NEL+2*NMT.
IWMAX is the amount of memory in MB.
The coarse mesh which covers the whole domain is presented in Figure 2.2(a), the part of the mesh around the obstacles on level 2 is present in Figure 2.2(b) and the part of the mesh around the obstacles on level 3 is present in Figure 2.2(c).

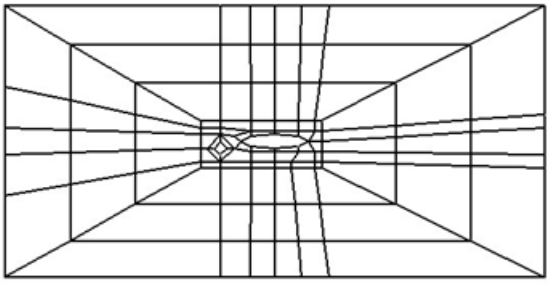

Fig.2.2(a) The coarse mesh (level 1)

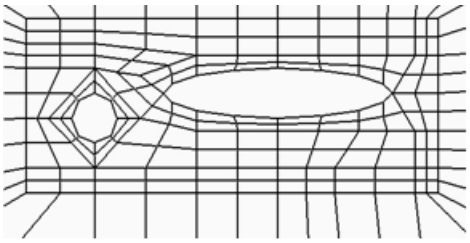

Fig.2.2(b) Mesh on level 2

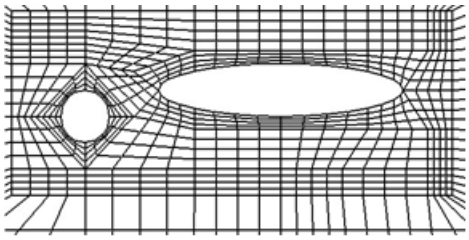

Fig. 2.2(c) Mesh on level 3.

2.4 Investigation of the accuracy of the solution:

The mesh refinement is needed to improve solution accuracy across the whole domain. We can control the relative accuracy of a solution to compare solutions on levels 3 - 7 with a solution on a finest mesh

(level 7). The table 2.2 shows the change in drag coefficient C_{drag} depending on the mesh refinement. The calculations were made for $Re = 10, \alpha = -5°$. Reference value C_{ref} is the drag coefficient of the ellipse on the finest mesh (level 7).

Table 2.2. The behaviour of drag coefficient C_{drag} of the ellipse according to computational levels for $Re = 10, \alpha = -5°$

Level	3	4	5	6	7
C_{drag}	1.0065	0.92601	0.90489	0.89996	0.89905
$(C_{drag}$-$C_{ref})/C_{ref}$	11.96%	3%	2.56%	0.66%	0.0%

2.5 Results and Conclusions

- The 2D steady incompressible, viscous flow past the circle and ellipse was investigated numerically.
- The numerical study has been carried out using the code cc2d which is the part of Featflow1.1 software.
- The magnitude of the uniform upstream velocity $|\mathbf{u}(U_x, U_y)|_\infty = 1$.
- The x-component of the upstream velocity $U_x \geq 0$.
- The problem has been solved over a range of Reynolds numbers $1 \leq Re \leq 100$ and the angle of attack of the upstream velocity $\alpha = -5°; 0°; 5°$.
- Drag force:
  a. Drag force decreases as Reynolds number increases due to influence of skin friction (Fig. 2.3).
  b. Drag force decreases as the angle of attack α increases (Fig. 2.3, Fig. 2.5).
- Lift Force:
  a. At positive small angles of attack $0° < \alpha \leq 5°$ the lift force decreases as Reynolds number increases (Fig. 2.4).
  b. At negative angles of attack $-5° \leq \alpha < 0°$ and $\alpha = 0°$ the lift force increases as Reynolds number increases (Fig. 2.4(b)).
- The effect of the interaction between obstacles was examined. It can be seen that the value of the drag forces acting on an isolated ellipse are larger than those obtained by corresponding simulations of flow past the cirle and the ellipse (Fig. 2.6-2.7).
- Flows patterns around the circle and ellipse are presented.
- The vortex structures were investigated. The phenomena of flow recirculation and separation in the rear of the obstacles are observed for $Re \geq 20$. The usual formation of clockwise and counter-clockwise vortex pairs take place (see Fig. 2.9-2.11).

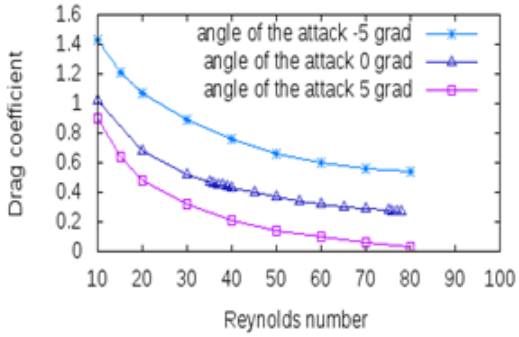

Fig.2.3 Variation of the drag coefficient with Reynolds number and angle of attack for the ellipse

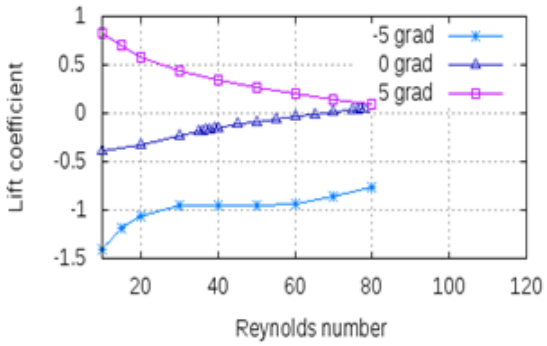

Fig.2.4 Variation of the lift coefficient with Reynolds number and angle of attack for the ellipse

- **Angle of attack $\alpha = -5°$, Fig. 2.9**
  Figure 2.10 shows magnified image in which we can see vortex formation between circle and ellipse. We can see that as Reynolds number increases velocity around obstacles also increases and streamlines becomes sharper.

- **Angle of attack $\alpha = 0°$, Fig. 2.10**
  In Figure 2.10 we can see that as Reynolds number increases velocity around obstacles also increases and streamlines becomes sharper and straight.

- **Angle of attack $\alpha = 5°$, Fig. 11**
  Figure 2.11 (a,b) shows Velocity magnitude plot at $Re = 10$ and $Re = 80$ respectively. We can see that as Reynolds number increases velocity around obstacles also increases and streamlines becomes sharper.

- At positive small angles of attack $0° \leq \alpha \leq 5°$ and $Re = 80$ the flow around two obstacles behaves like if this group of obstacles formed only one large obstacle. The both obstacles behave more like one streamline surface (see Fig 2.12 a, b).

- At $\alpha = -5°$, the both obstacles behave more like a single obstacle (Fig 2.12 c).

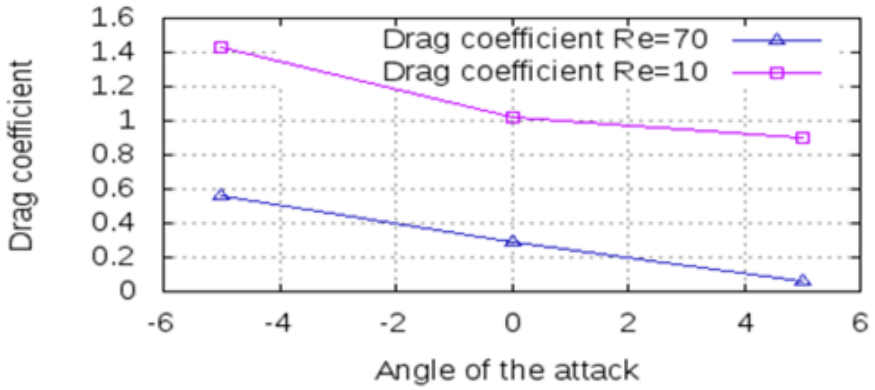

Fig.2.5 Variation of the drag coefficient of the ellipse with the angle of attack $-5^\circ \leq \alpha \leq 5^\circ$ and $Re = 10, 70$.

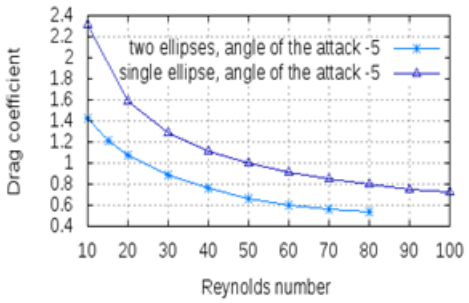

(a) Drag coefficient at $\alpha = -5^\circ$

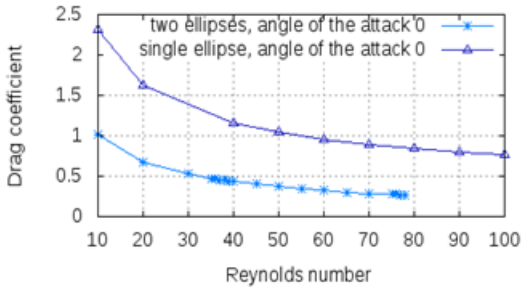

(b) Drag coefficient at $\alpha = 0^\circ$

Fig.2.6 Variation of drag coefficient of ellipse with the different Reynolds numbers at the angle of attacks $\alpha = -5^\circ$ (a) and $\alpha = 0^\circ$ (b)

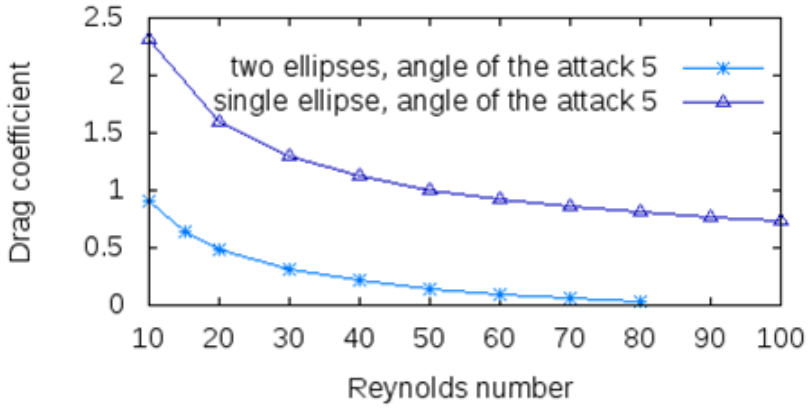

Fig.2.7 Drag coefficient of an isolated ellipse and Drag coefficient of an ellipse obtained by corresponding simulation of flow past two obstacles at different Re and $\alpha = 5^\circ$

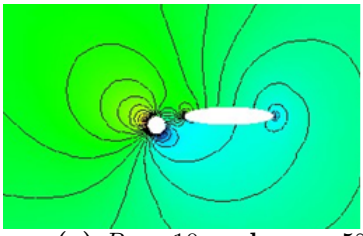

(a) $Re = 10$ and $\alpha = -5°$

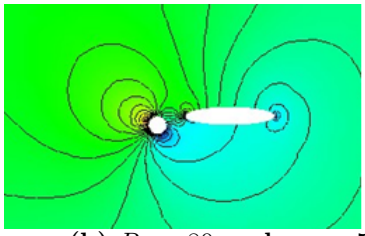

(b) $Re = 80$ and $\alpha = -5°$

Fig.2.8 Pressure plot

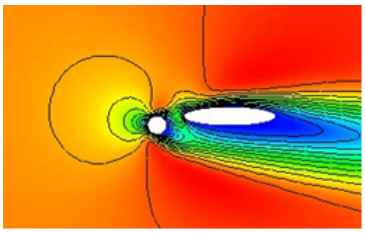

(a) $Re = 10$ and $\alpha = -5°$

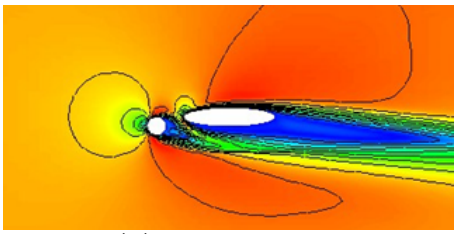

(b) $Re = 80$ and $\alpha = -5°$

Fig.2.9 Velocity magnitude plot

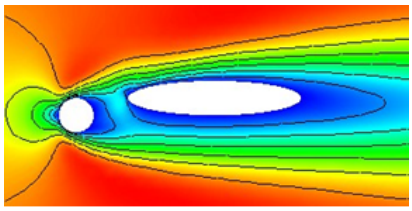

(a) $Re = 10$ and $\alpha = 0°$

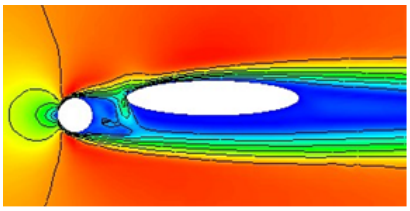

(b) $Re = 80$ and $\alpha = 0°$

Fig.2.10 Velocity magnitude plot

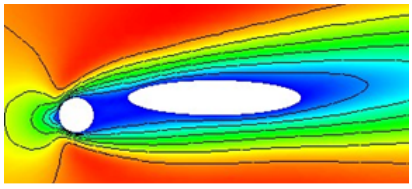

(a) $Re = 10$ and $\alpha = 5°$

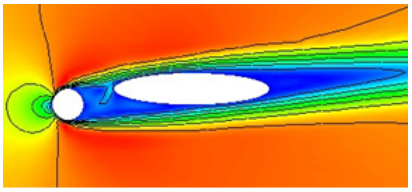

(b) $Re = 80$ and $\alpha = 5°$

Fig.2.11 Velocity magnitude plot

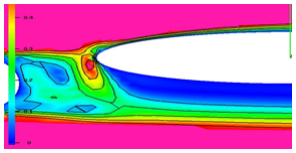

(a) $\alpha = 0°$

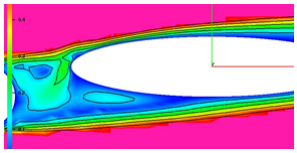

(b) $\alpha = 5°$

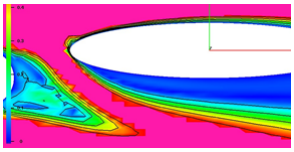

(c) $\alpha = -5°$

Fig.2.12 Velocity magnitude plot around the ellipse at $Re = 80$

3 Task III

Title: Numerical study of flow across a circle, an ellipse and a rectangle placed in succession in a uniform stream of infinite extent. The x-component of the upstream velocity $U_x \geq 0$.

Submitted by:

- Prabhat Ranjan Bhat (146078)
- Vikram Bangalore Nagendra (146062)
- Sankaranarayanan Subramanian (146094)

Aim

- Examine a two-dimensional low Reynolds number flow around the ellipse, the circle and the rectangle immersed in a uniform stream of infinite extent (see Fig.3.1).
- The x-component of the upstream velocity $U_x \geq 0$.
- The magnitude of the uniform upstream velocity $|\mathbf{u}(U_x, U_y)|_\infty = U_\infty = 1$.
- Solve the problem for different angle of attack of the upstream velocity $\alpha = -5°; 0°; 5°$ and Reynolds number $1 \leq Re \leq 100$
- Analyse the resulting drag and lift forces acting on obstacles with respect to the angle of attack of the upstream velocity and Reynolds number.
- Determine the influence of the circle and the rectangle onto the resulting drag and lift coefficients of the ellipse.

3.1 Computational domain

- **The exterior geometry of the rectangle:**
  $h = 40.0,\ l = 80.0$ - height and width of the bounding box.
  $C(0.0, 0.0)$ is the position of the center of the rectangle.
  $(-40.0, -20.0)$ is the point of the left lower corner of the box.
  $(40.0, 20.0)$ is the point of the right upper corner of the box.
- **Position of the ellipse (boundary 2):**
  $h1 = 2.0,\ l1 = 10.0$ - height and width of the ellipse.
  $C(0.0, 0.0)$ is the position of the center of the ellipse.
  $E = 5$ is the aspect ratio of the ellipse ($E = l1/h1$).
- **Position of the circle(boundary 3):**
  $R = 0.5$ is the radius of the square with its center at $C(-8.0, -1.0)$.

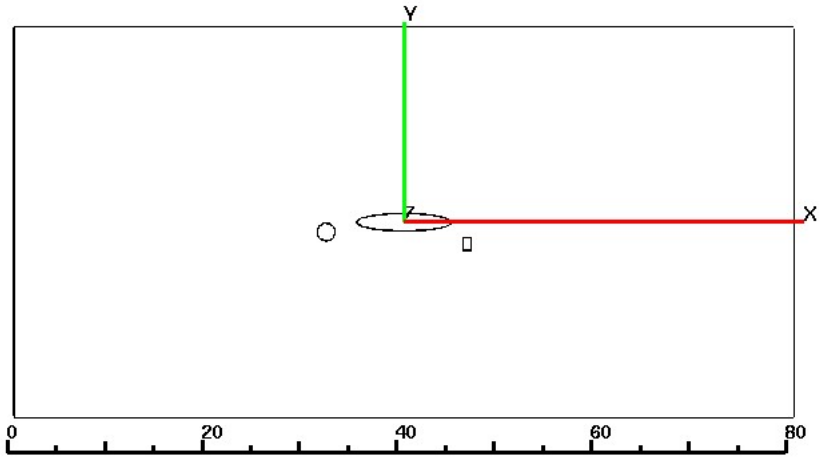

3.1 Computational Domain

- **Position of the rectangle (boundary 4):**
  $h2 = 1.5.0,\ l2 = 1.0$ - height and width of the rectangle.
  $C(6.5, -2.25)$ is the position of the center of the rectangle.

3.2 Implementation of Boundary conditions

- **Case** $\alpha = 0^0$

  Upstream entrance (the Dirichlet boundary conditions):

  $U_x = 1.0, U_y = 0.0$ on the line: $x = -40.0$; $-20.0 \leq y \leq 20.0$.

  Downstream exit (Do nothing's boundary conditions):

  on the line: $-40.0 \leq x \leq 40.0$; $y = 20.0$.

  on the line: $-40.0 \leq x \leq 40.0$; $y = -20.0$.

  on the line $x = 40.0$; $-20.0 \leq y \leq 20.0$.

- **Case** $\alpha = -5^\circ$

  Upstream entrance (the Dirichlet boundary condition):

  $U_x = \cos(\alpha), U_y = \sin(\alpha)$ on the line: $x = -40.0$; $-20.0 \leq y \leq 20.0$.

  $U_x = \cos(\alpha), U_y = \sin(\alpha)$ on the line: $-40.0 \leq x \leq 40$; $y = 20.0$.

  Downstream exit (Do nothing's" boundary conditions):

  on the line: $-40.0 \leq x \leq 40.0$; $y = -20.0$.

  on the line: $x = 40.0$; $-20.0 \leq y \leq 20.0$.

- **Case** $\alpha = 5^\circ$

Upstream entrance (the Dirichlet boundary condition) :

$U_x = \cos(\alpha), U_y = \sin(\alpha)$ on the line: $x = -40.0$; $-20 \leq y \leq 20$.

$U_x = \cos(\alpha), U_y = \sin(\alpha)$ on the line: $-40.0 \leq x \leq 40.0$; $y = -20.0$.

Downstream exit (Do nothing's boundary conditions):

on the line:$-40.0 \leq x \leq 40.0$; $y = 20.0$.

on the line: $x = 40.0$; $-20.0 \leq y \leq 20.0$.

3.3 Spatial Discretization, Mesh refinement and Computational requirements in the code cc2d

We perform series of calculations on different solution levels: 3 - 7. Information about mesh refinement, memory capacity and computational time (Total Time) is available in the protocol file. Table 3.1 presents the progression of grid sizes through seven levels and the typical computational requirement.

Table 3.1 Mesh refinement and computational requirements.

Level	NEL	NMT	d.o.f	IWMAX	Total Time
Lev 1: coarse mesh	101	221	543	0.064MB	0.06sec
Lev 5 : mesh	25.856	52.016	129.888	19.67MB	30.51sec
Lev 7 : finest mesh	413.696	828.608	2.070.912	313.82MB	1632.07sec

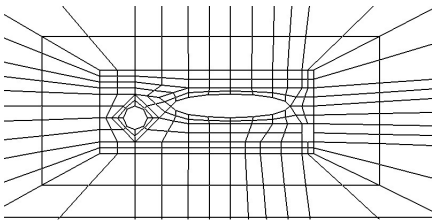

Fig.3.2 Mesh on level 2

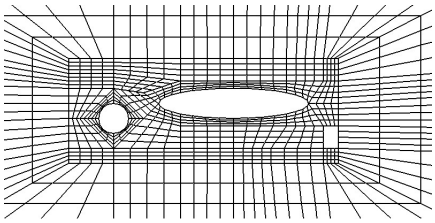

Fig.3.3 Mesh on level 3

NEL is the total number of cells associated with pressure unknowns.

NMT is the total number of midpoints of edges associated with x- and y- components velocity unknowns.

Degrees of freedom d.o.f.'s is expressed by NEL+2*NMT.

IWMAX is the amount of memory in MB.
The coarse mesh which covers the whole domain is presented in figure 3.2, the part of the mesh around the obstacles on level 2 is present in figure 3.2 and the part of the mesh around the obstacles on level 3 is present in figure 3.3.

3.4 Investigation of the accuracy of the solution:

The mesh refinement is needed to improve solution accuracy across the whole domain. We can control the relative accuracy of a solution to compare solutions on levels 3, 4, 5, 6, 7 with a solution on a finest mesh (level 7). The table 3.2 shows the change in drag coefficient C_{drag} depending on the mesh refinement. The calculations were made for $Re = 10, \alpha = -5°$. Reference value C_{ref} is the drag coefficient of the ellipse on the finest mesh (level 7).

Table 3.2. The behaviour of drag coefficient C_{drag} of the ellipse according to computational levels for $Re = 10, \alpha = -5°$

Level	3	4	5	6	7
C_{drag}	0.99582	0.93999	0.92437	0.92109	0.92114
$(C_{drag}$-$C_{ref})/C_{ref}$	8.1%	2.05%	0.35%	0.001%	0.0%

3.5 Results and Discussions

- The 2D steady incompressible, viscous flow past the circle, ellipse and rectangle was investigated numerically.
- The numerical study has been carried out using the code cc2 from Featflow1.1 software.
- The magnitude of the uniform upstream velocity $|\mathbf{u}(U_x, U_y)|_\infty = 1$.
- The x-component of the upstream velocity $U_x \geq 0$.
- The problem has been solved over a range of Reynolds numbers $1 \leq Re \leq 100$
  and the angle of attack of the upstream velocity $\alpha = -5°; 0°; 5°$.
- Drag force:
  a. Drag force decreases as Reynolds number increases (Fig. 3.4).
  b. Drag force decreases as the angle of attack α increases (Fig. 3.4).
- Lift Force:
  a. At positive small angle of attack $0° \leq \alpha \leq 5°$ the lift coefficient of ellipse decreases as Reynolds number increases (Fig. 3.5).
  b. At angles of attack $\alpha = 0°$ and for $Re \geq 30$ we observe that the lift force can be neglected.

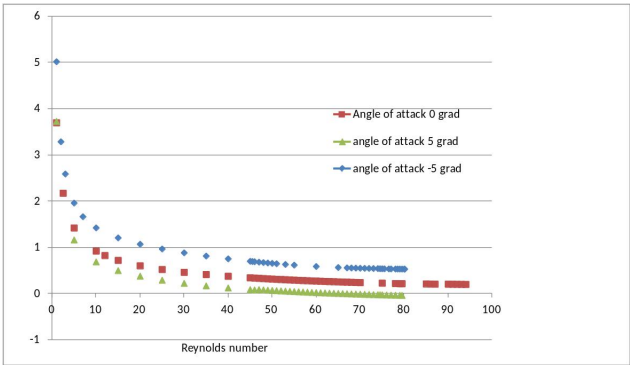

Fig.3.4 Variation of drag coefficient of the ellipse with different Re and angle of attacks

- The effect of the interaction between obstacles was examined. It can be seen that the value of the drag forces acting on an isolated ellipse are larger than those obtained by corresponding simulations of flow past three obstacles (Figures 3.6 (a-b)).

- Flows patterns around the obstacles are presented.

- The vortex structures were investigated. The phenomena of flow recirculation and separation in the rear of the both cylinders are observed for $Re \geq 20$. The usual formation of clockwise and counter-clockwise vortex pairs take place.

- **Angle of attack $\alpha = -5°$, Fig. 3.8**
  Figure 3.8 shows velocity magnified image at $Re = 10; 80$. We can see vortex formation between the circle and the ellipse. Velocity around obstacles increases and streamlines becomes sharper as Reynolds number increases. The ellipse and rectangle behave more like one streamline surface as Reynolds number decreases (Figures 3.8(a)).

- **Angle of attack $\alpha = 0°$, Fig. 3.9**
  Figure 3.9 shows velocity magnified image at $Re = 10; 80$. Streamlines become straight as Reynolds number increases. We can see vortex formation between the circle, the ellipse and the rectangle.

- **Angle of attack $\alpha = 5°$, Fig. 3.10**
  Figure 10 shows velocity magnified image at $Re = 10; 80$. Velocity around obstacles increases and streamlines becomes sharper as Reynolds number increases. The flow around the obstacles becomes very copmlex.

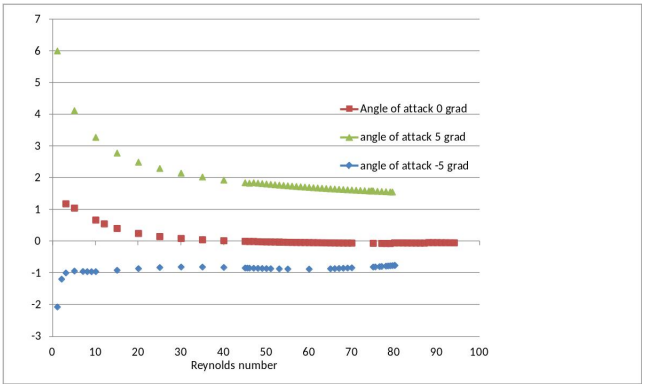

Fig.3.5 Variation of lift coefficient of the ellipse with different Re and angle of attacks

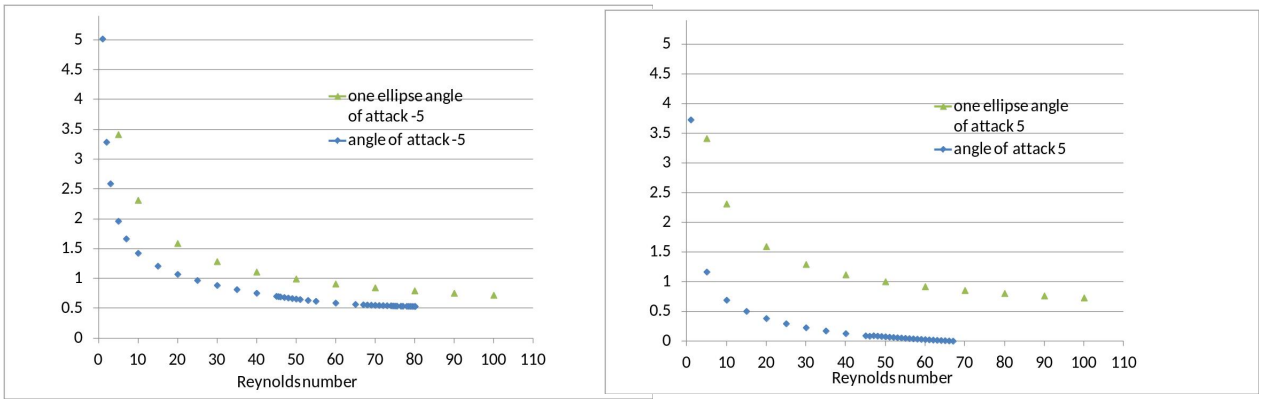

a. $\alpha = -5^\circ$ **b.** $\alpha = 5^\circ$

Fig.3.6 Drag coefficient of an isolated ellipse and Drag coefficient of an ellipse obtained by corresponding simulation of flow past two obstacles at different Re and $\alpha = -5^\circ$ (a) and $\alpha = 5^\circ$ (b)

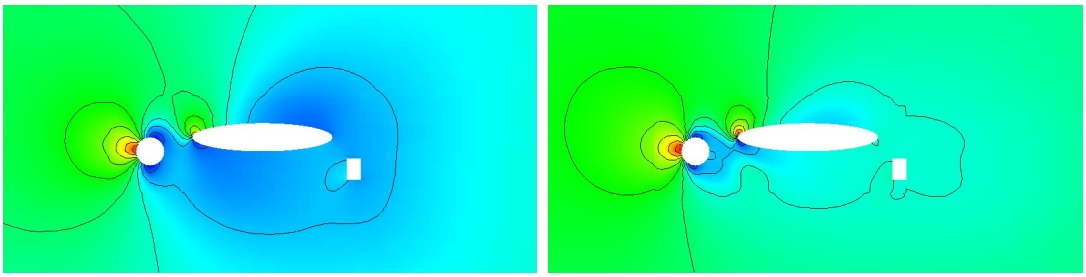

(a) $Re = 10$ **and** $\alpha = -5^\circ$ **(b)** $Re = 80$ **and** $\alpha = -5^\circ$

Fig.3.7 Pressure plot

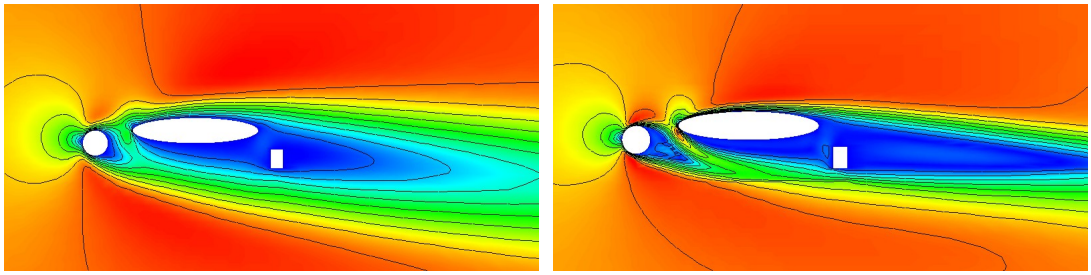

(a) $Re = 10$ **and** $\alpha = -5°$ **(b)** $Re = 80$ **and** $\alpha = -5°$

Fig.3.8 Velocity magnitude plot

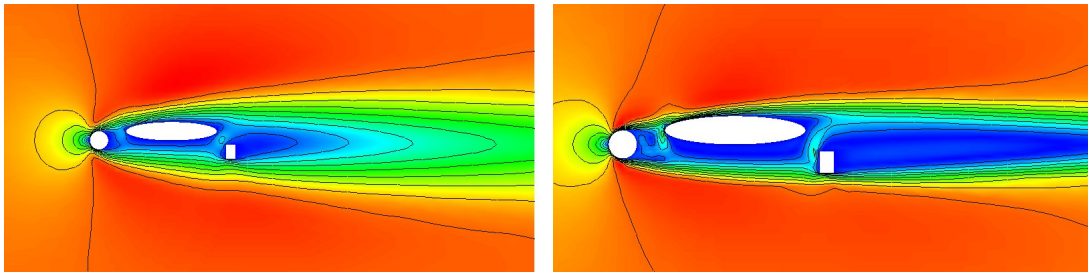

(a) $Re = 10$ **and** $\alpha = 0°$ **(b)** $Re = 80$ **and** $\alpha = 0°$

Fig.3.9 Velocity magnitude plot

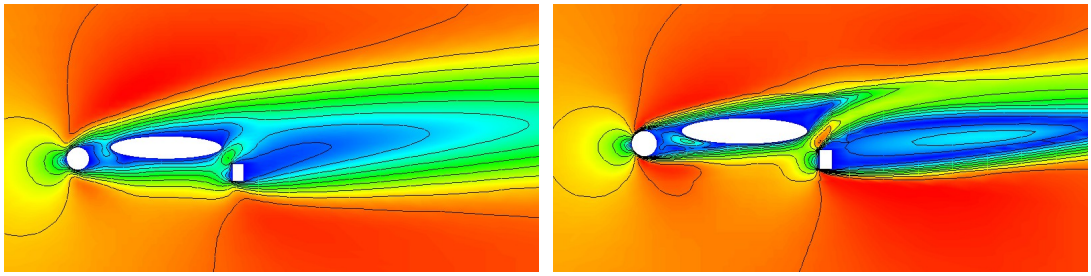

(a) $Re = 10$ **and** $\alpha = 5°$ **(b)** $Re = 80$ **and** $\alpha = 5°$

Fig.3.10 Velocity magnitude plot

4 Task IV

Title: Numerical study of formation of vortex field in two successive ellipses placed in a uniform stream of infinite extends.

Submitted by:

- Provodin Artem
- Alberto Morales San Juan

Aim

- Examine a two-dimensional low Reynolds number flow around two ellipses in succession immersed in a stream of infinite extent (see Fig.4.1).
- The x-component of the upstream velocity $U_x \geq 0$.
- The magnitude of the uniform upstream velocity $|\mathbf{u}(U_x, U_y)|_\infty = U_\infty = 1$.
- Study the problem for Reynolds number in the range $1 \leq Re \leq 100$ and the angle of attack of the upstream velocity at $\alpha = -5°; 0°; 5°$.
- Analyse the resulting drag and lift forces acting on obstacles with respect to the angle of attack of the upstream velocity and the Reynolds number.
- Determine the influence of the small eplipse onto the resulting drag and lift coefficients of the large ellipse.

4.1 Computational Domain

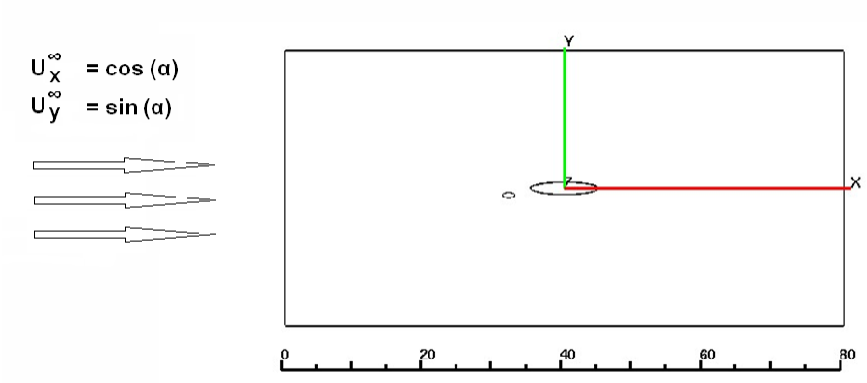

Fig.4.1 Computational Domain

- **The exterior geometry of the rectangle:**
  $h = 40$, $l = 80$ - height and width of the bounding box.
  $C(0.0, 0.0)$ is the position of the center of the rectangle.
  $(-40.0, -20.0$ is the point of the left lower corner of the box.
  $(40.0, 20.0)$ is the point of the right upper corner of the box.

- **Position of the large ellipse (boundary 2):**
  $h1 = 2$, $l1 = 10.0$ - height and length of the ellipse:
  $C(0.0, 0.0)$ is the position of the center of the ellipse.
  $E = 5$ is the aspect ratio of ellipse ($E = l1/h1$).

- **Position of the small ellipse (boundary 3):**
  $h2 = 1$, $l2 = 2.0$ - height and length of the ellipse:
  $C(-8.0, -1.0)$ is the position of the center of the ellipse.
  $E = 2$ is the aspect ratio of ellipse ($E = l2/h2$).

4.2 Implementation of Boundary conditions

- **Case** $\alpha = 0^0$

  Upstream entrance (the Dirichlet boundary conditions):

  $U_x = 1.0, U_y = 0.0$ on the line: $x = -40.0$; $-20.0 \leq y \leq 20.0$.

  Downstream exit (Do nothing's boundary conditions):

  on the line: $-40.0 \leq x \leq 40.0$; $y = 20.0$.

  on the line: $-40.0 \leq x \leq 40.0$; $y = -20.0$.

  on the line $x = 40.0$; $-20.0 \leq y \leq 20.0$.

- **Case** $\alpha = -5^\circ$

  Upstream entrance (the Dirichlet boundary condition):

  $U_x = \cos(\alpha), U_y = \sin(\alpha)$ on the line: $x = -40.0$; $-20.0 \leq y \leq 20.0$.

  $U_x = \cos(\alpha), U_y = \sin(\alpha)$ on the line: $-40.0 \leq x \leq 40$; $y = 20.0$.

  Downstream exit (Do nothing's" boundary conditions):

  on the line: $-40.0 \leq x \leq 40.0$; $y = -20.0$.

  on the line: $x = 40.0$; $-20.0 \leq y \leq 20.0$.

- **Case** $\alpha = 5^\circ$

  Upstream entrance (the Dirichlet boundary condition) :

  $U_x = \cos(\alpha), U_y = \sin(\alpha)$ on the line: $x = -40.0$; $-20 \leq y \leq 20$.

  $U_x = \cos(\alpha), U_y = \sin(\alpha)$ on the line: $-40.0 \leq x \leq 40.0$; $y = -20.0$.

Downstream exit (Do nothing's boundary conditions):

on the line:$-40.0 \leq x \leq 40.0$; $y = 20.0$.

on the line: $x = 40.0$; $-20.0 \leq y \leq 20.0$.

4.3 Spatial Discretization, Mesh refinement and Computational requirements in the code cc2d

We perform series of calculations on different solution levels: 3,4,5,6,7. Table 4.1 presents the progression of grid sizes through seven levels and the typical computational requirement.

Information about mesh refinement, memory capacity and computational time (Total Time) is available in the protocol file.

Table 4.1. Mesh refinement and computational requirements.

Level	(NEL)	(NMT)	d.o.f	IWMAX	Time
Lev 1: coarse mesh	58	133	324	0.038MB	0.03sec
Lev 5:	14.848	29.968	74.784	11.23MB	37.59sec
Lev 7: finest mesh	237.568	476.224	1.190.016	178.616 MB	1180.35sec

NEL is the total number of cells associated with pressure unknowns.

NMT is the total number of midpoints of edges associated with x- and y- components velocity unknowns.

Degrees of freedom d.o.f.'s is expressed by NEL+2*NMT.

IWMAX is the amount of memory in MB.

The coarse mesh which covers the whole domain is presented in Figure 4.2, the part of the mesh around the obstacles on level 2 - Figure 4.3(a) and on level 3 - Figure 4.3(b).

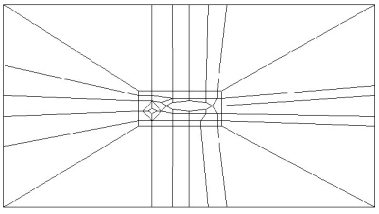

Fig.4.2 The coarse mesh (level 1)

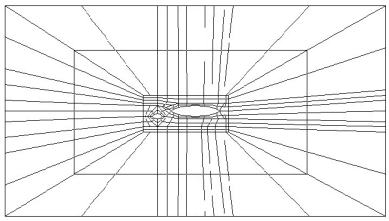

Fig.4.3(a) Mesh on level 2

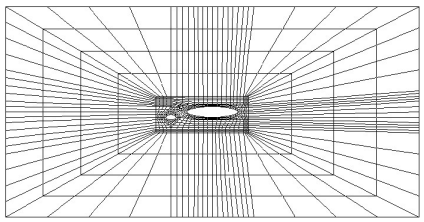

Fig.4.3(b) Mesh on level 3.

4.4 Investigation of the accuracy of the solution:

The mesh refinement is needed to improve solution accuracy across the whole domain. We can control the relative accuracy of a solution to compare solutions on levels 3, 4, 5, 6, 7 with a solution on a finest mesh (level 7). The table 4.2 shows the change in drag coefficient C_{drag} depending on the mesh refinement. The calculations were made for $Re = 10, \alpha = -5°$. Reference value C_{ref} is the drag coefficient of the large ellipse on the finest mesh (level 7).

Table 4.2. The behaviour of drag coefficient C_{drag} of the large ellipse according to computational levels for $Re = 10, \alpha = -5°$

Level	3	4	5	6	7
C_{drag}	1.5018	1.4454	1.397	1.3752	1.3732
$(C_{drag} - C_{ref})/C_{ref}$	9.37%	5.27%	1.74%	0.15%	0.0%

4.5 Results and Conclusions

The problem has been solved for $\alpha = -5°; 0°; 5°$ and different Reynolds numbers $1 \leq Re \leq 100$. We investigated forces acting on the large ellipse (downstream obstacle) with respect to the Reynolds number Re and the angle of attack α of the upstream velocity.

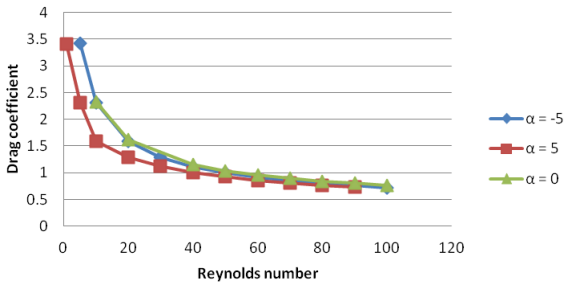

Fig.4.4 The drag coefficients for $\alpha = -5°, \alpha = 5°, \alpha = 0°$.

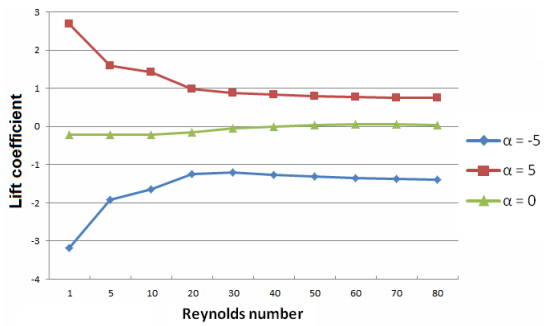

Fig.4.5 The lift coefficients for $\alpha = -5°, \alpha = 5°, \alpha = 0°$.

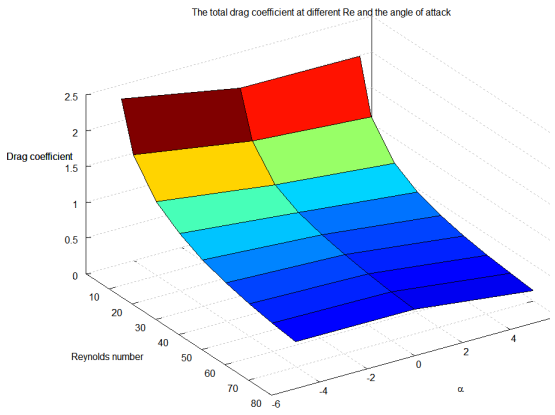

Fig.4.6 (a) Drag coefficient in 3D

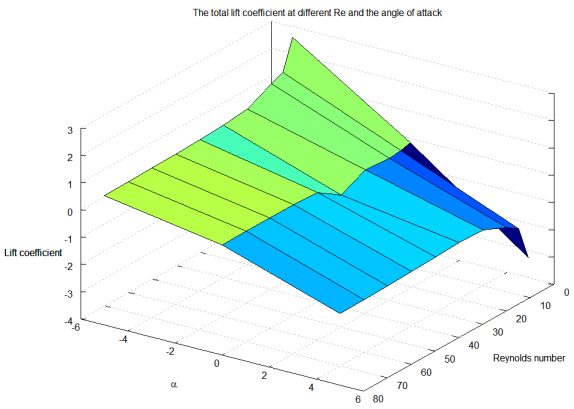

Fig.4.6 (b) Lift coefficient in 3D

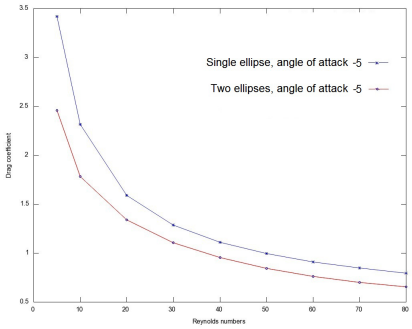

(a) $\alpha = -5°$

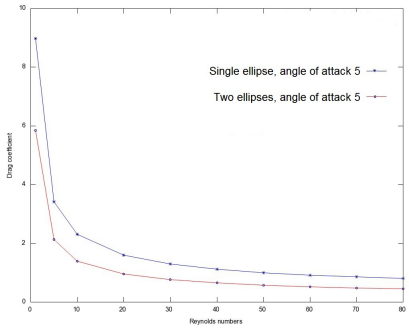

(b) $\alpha = 0°$

Fig.4.7 Drag coefficient of an large isolated ellipse and Drag coefficient of that obtained by corresponding simulation of flow past two obstacles for different Re and α

- The 2D steady incompressible, viscous flow past two ellipses was investigated numerically.
- The numerical study has been carried out using the code cc2d which is the part of Featflow1.1 software.
- The magnitude of the uniform upstream velocity $|\mathbf{u}(U_x, U_y)|_\infty = 1$.
- The x-component of the upstream velocity $U_x \geq 0$.
- The problem has been solved over a range of Reynolds numbers $1 \leq Re \leq 100$ and the angle of attack of the upstream velocity $\alpha = -5°; 0°; 5°$.
- Drag force:
  a. Drag force decreases as Reynolds number increases (see Fig. 4.4, Fig. 4.6a).
  b. Drag force decreases as the angle of attack α increases (see Fig. 4.4).

- Lift force:
  a. The lift coefficient varies significantly with angle of the attack (see Fig. 4.5, Fig. 4.6b):
  b. In the case $\alpha = 0$ the lift coefficient converges very rapidly to 0 as Reynolds number increases.
  c. In the case $\alpha = 5^\circ$ the lift coefficient decreases as Reynolds number increases.
  d. In the case $\alpha = -5^\circ$ the lift coefficient varies depend on Reynolds number.

- The effect of the interaction between obstacles was examined. It can be seen that the value of the drag forces acting on an isolated ellipse are larger than those obtained by corresponding simulations of flow past two cylinders (Figure 4.7).

- Flows patterns around two ellipses are presented.

- The vortex structures were investigated. The phenomena of flow recirculation and separation in the rear of the both ellipses are observed for $Re \geq 20$. The usual formation of clockwise and counter-clockwise vortex pairs take place.

- **At angle of attack** $\alpha = -5^\circ$
  ¿From figure 4.8 we can see that as Reynolds number increases velocity around obstacles also increases and streamlines becomes sharper. As the angle of attack is negative flow converges in downwards. Figure 8 shows magnified image in which we can see vortex formation between the ellipses.

- **At angle of attack** $\alpha = 0^\circ$
  ¿From Velocity magnitude plot (Figure 4.9) we can see that as Reynolds number increases velocity around obstacles also increases and streamlines becomes sharper. As angle of attack is 0° flow is straight.

- **At angle of attack** $\alpha = 5^\circ$
  Figure 4.10 shows Velocity magnitude plot at the angle of attack $\alpha = 5^\circ$. We can see that as Reynolds number increases velocity around obstacles also increases and streamlines becomes sharper.

- At low Reynolds number $Re = 5$ and $0^\circ \leq \alpha \leq 5^\circ 5$ (see Fig. 4.8(a), 4.9(a), 4.10(a)) the flow around two obstacles behaves like if this group of obstacles formed only one large obstacle and both obstacles behave more like one streamline surface.

- It is seen from Figure 4.8(b) that for higher Reynolds number $Re = 40$ and the negative angle of attack $\alpha = -5^\circ$ the both ellipses behave more like a single obstasle.

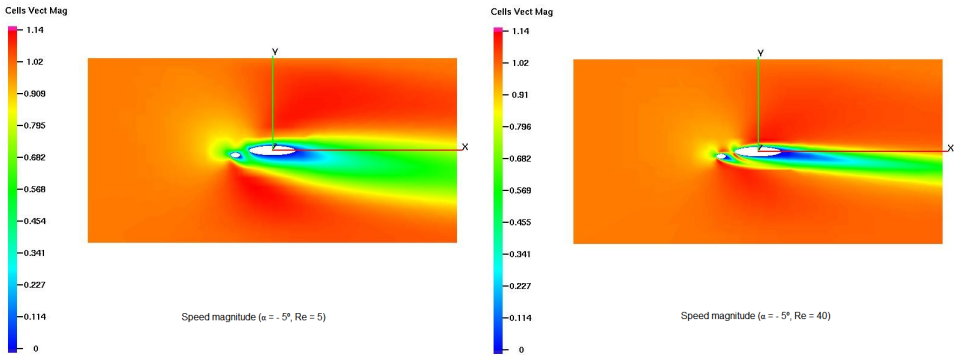

(a) $Re = 5$ **and** $\alpha = -5°$ **(b)** $Re = 40$ **and** $\alpha = -5°$

Fig.4.8 Velocity magnitude plot.

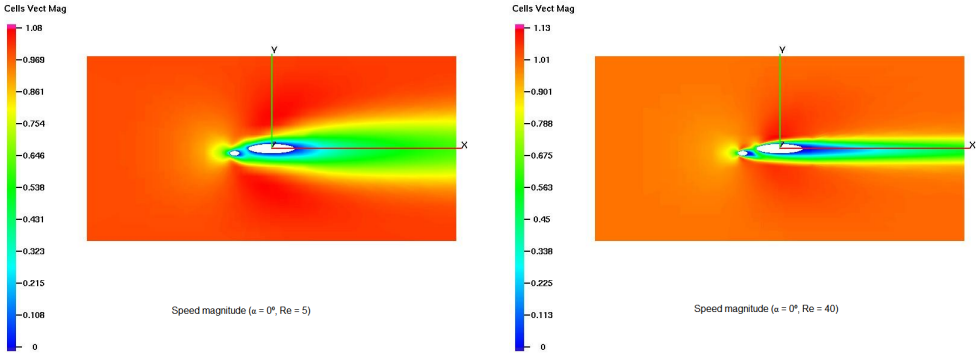

(a) $Re = 5$ **and** $\alpha = 0°$ **(b)** $Re = 40$ **and** $\alpha = 0°$

Fig.4.9 Velocity magnitude plot.

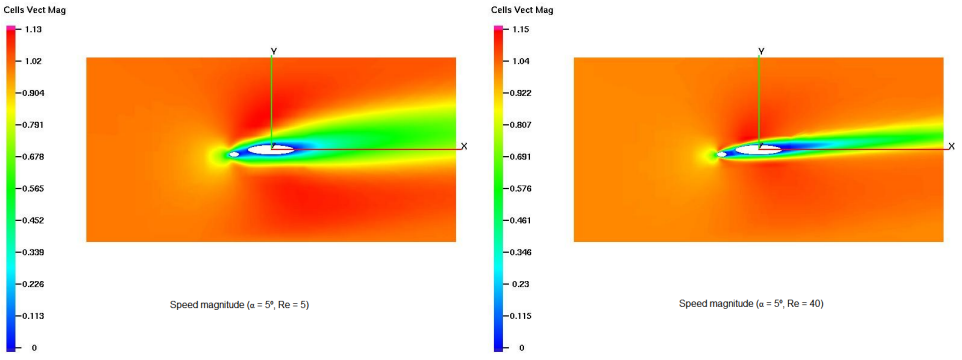

(a) $Re = 5$ **and** $\alpha = 5°$ **(b)** $Re = 40$ **and** $\alpha = 5°$

Fig.4.10 Velocity magnitude plot.

5 Task V

Title: TA2: Inverse or optimization problems for multiple (ellipse)ellipsoid configuration.
Submitted by Jyril

- **Keywords**
  Inverse problems, shape recovery, CFD, electromagnetics, acoustics.
- **Requirements** Navier-Stokes solver, Maxwell solver, Acoustics solver, Mesher

5.1 Objectives

- **Aerodynamic reconstruction problem**
  Recovery of the original position of two ellipses (2D) or ellipsoids (3D)using potential, Euler, or Navier Stokes flows for $Re = 100$ and $Re = 500$.
- **Radar wave problem**
  Reconstruction of the original position of ellipses/ellipsoids using radar cross subsection with perfectly conducting material.
- **Acoustics problem**
  Reconstruction of the original position of ellipses/ellipsoids using acoustic waves.

5.2 Computational domain

See the figure 5.1 for 2D case

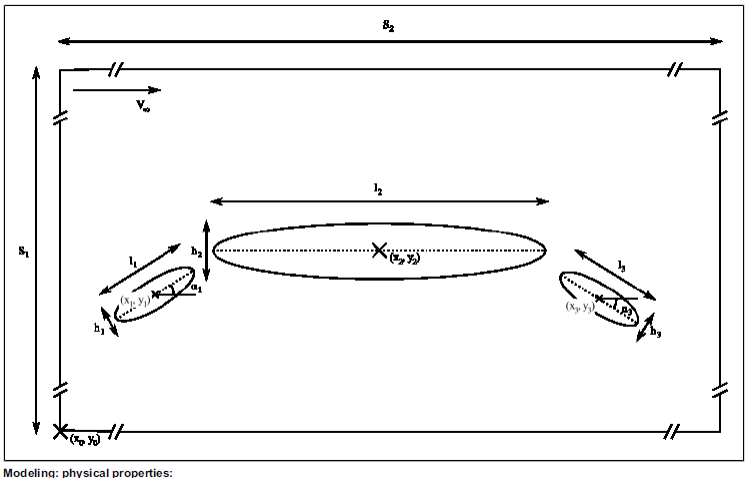

5.1 Illustration of Computational Domain

- **The exterior geometry of the bounding box:**
  $s_1 = s_3 = 40$ height and width of the bounding box(aerodynamic reconstruction problem).
  $s_1 = s_3 = 20$ height and width of the bounding box(radar wave/acoustics problem).
  $s_2 = 80$ length of the bounding box(aerodynamic reconstruction problem).
  $s_2 = 30$ length of the bounding box (radar wave/acoustics problem).
  $(x_0, y_0, z_0) = (-30, -20, -20)$ front lower corner of the bounding box (aerodynamic reconstruction problem).
  $(x_0, y_0, z_0) = (-15, -10, -10)$ front lower corner of the bounding box (radar wave/acoustics problem).

- **Position of ellipse/ellipsoid 1**
  $l_1 = 2.0$ length of ellipse/ellipsoid 1.
  $h_1 = w_1 = 0.5$ height and width of ellipse/ellipsoid 1.
  $(x_1, y_1, z_1) = (-7, -0.5, 0)$ reference position of the ellipse/ellipsoid 1.
  $\alpha_1 = -3^\circ$ reference angle of the ellipse/ellipsoid 1.

- **Position of ellipse/ellipsoid 2**
  $l_2 = 10.0$ length of ellipse/ellipsoid 2.
  $h_2 = w_2 = 1.0$ height and width of ellipse/ellipsoid 2.
  $(x_2, y_2, z_2) = (0, 0, 0)$ reference position of the ellipse/ellipsoid 2.
  $\alpha_2 = 0^\circ$ reference angle of the ellipse/ellipsoid 2.

- **Position of ellipse/ellipsoid 3**
  $l_3 = 3.5$ length of ellipse/ellipsoid 3.
  $h_3 = w_3 = 0.5$ height and width of ellipse/ellipsoid 3.
  $(x_3, y_3, z_3) = (7.5, -0.5, 0)$ reference position of the ellipse/ellipsoid 3.
  $\alpha_3 = 3^\circ$ reference angle of the ellipse/ellipsoid 3.

5.3 Modeling

- **Aerodynamic reconstruction problem**
  Incompressible fluid(Navier-Stokes laminar flow)
  Kinematic viscosity $\nu = 1/10$ or $\nu = 1/50$
  Reynolds number $Re = \frac{\nu_\infty l_2}{\nu}, Re = 100, 500.$

- **Radar wave/acoustics problem**
  Density $\rho = 1$.

Radar wave: $f = 0.6GHz$ and $\lambda = 0.5m$

Acoustics wave: $\lambda = 0.5m$.

5.4 Boundary and initial conditions for computations

- **Aerodynamic reconstruction problem**

  Upstream entrance: $v_x = \cos\alpha$, $v_y = \sin\alpha$

  Angle of attack: $\alpha = 5^\circ$

  downstream exit: free boundary conditions

  Ellipse/ellipsoid surface: no-slip condition.

- **Radar wave/acoustics problem**

  Monostatic radar

  Angle of radar illumination 0°

  Outer boundary: absorbing boundary condition at infinity(Enquist)

  Ellipse surface: perfectly conducting material.

- **Material Parameters**

  Fluid

- **Optimization**

  Aerodynamic reconstruction problem: Reconstruction of the target pressure on the surface of the ellipses.

  Radar wave/acoustics problem: Recovery of the target radar cross subsection /scattering cross subsection.

  The target vector is $x^* = x_1, y_1, \alpha_1, x_3, y_3, \alpha_3 = -7, -0.5, -3.0^\circ, 7.5, -0.5, 36\circ$.

- **Design parameters**

  - Position of ellipse 1:

    $-10 \leq x_1 \leq -6.5$

    $-1.5 \leq y_1 \leq 0.0$

  - Clockwise angle of ellipse 1:

    $-10 \leq \alpha_1 \leq 0$

  - position of ellipse 3:

    $7.25 \leq x_3 \leq 10.0$

    $-1.5 \leq y_3 \leq 0.0$

  - clockwise position of ellipse 3:

    $0.0 \leq \alpha_3 \leq 10.0$

    in addition, the ellipse/ellipsoids must not be overlapping.

5.5 Aerodynamic reconstruction problem

$$minf = f_1 + f_2 + f_3$$

where f and L^2 error norm of the surface pressure:

$$f_1 = \int_{r_1} \mid p_1 - p_1^* \mid^2$$
$$f_2 = \int_{r_2} \mid p_2 - p_2^* \mid^2$$
$$f_3 = \int_{r_3} \mid p_3 - p_3^* \mid^2$$

where p_i and p_i^* the target pressure on the surface of the ellipse i.

5.6 Radar wave/Acoustics problem

$$min \int_\zeta \mid u_\infty - u_\infty^* \mid^2 d\zeta$$

where ζ is the direction of the reflected wave, u_∞ and u_∞^* are the field patterns for the computed case and the target respectively.

5.7 Results

- Target mesh and the mesh of the best solution in Paraview Compatible format.
- Target geometry compared to the best solution(list of boundary points coordinates)
- The optimized design variable values
- **Aerodynamics Reconstruction Problem**
  Pressure coefficient of the target compared to the best solution(list of points)
  Pressure and the velocity field of the target and the best solution in the Paraview compatible format.
- **Radar wave/Acoustics Problem**
  Radar cross subsection/scattering cross subsection of the best solution compared to the target(list of values from 0° to 360°)
  Scatter field of the target and the best solution(imaginary and real component) in Paraview compatible format.
- For the tested algorithms the average convergence of the tested algorithms over 10 runs is required (a table of increasing number of fitness evaluation on the first column, objective function values on the second column).
- In addition, the following information is needed:
  Mean final value

Standard deviation of the final values

Minimum final value

Maximum final value

Average number of fitness calculations required.

5.8 Computation Results

- Assessment of error in the quality of interest (QoI) for radar wave problem.
- Inverse problem for Multiple Ellipse Configuration using Global Meta-model based on optimization.
- Recovery of positions in Navier-Stokes flow $Re = 100$ using SACPDE and Hooke-Jeeves pattern search.
- Recovery of positions in Navier-Stokes flow $Re = 500$ using Hooke-Jeeves pattern search.
- Recovery of position in potential flow using GAs and pattern search.
- TA2 test case using Famosa.

References

[1] G. P. Galdi, M. Heywood, R. Rannacher. Fundamental directions in Mathematical Fluid Mechanics. Basel, Bogton, Berlin, Birkhäuers, 2000.

[2] S.Turek, Chr. Becker. FEATFLOW, Finite Element Software For The Incompressible Navier-Stokes Equations User Manual 1.1. Heidelberg, 02.01.1998.

[3] H.M.Badr, S.C.R. Dennis, Serpil Kocabiyik. Numerical simulation of the unsteady flow over an elliptical cylinder at different orientations. Int.J.Numer.Meth.fluids 2011, 37:05-931.

[4] P. Sivakumar, Ram Prakash Bharti, R.P. Chhabra. Steady flow of power-law fluids across an unconfined elliptical cylinder. Chemical Engineering Science 62 (2007), pp. 1682-1702.

[5] S.A. Johnson, M.C. Thompson and K. Hourigan. Flow Past Elliptical Cylinders at low Reynolds Number. 14th Australasian Fluid Mechanics Conference Adelaide University, Adelaide, Australia 10-14 December 2001.

[6] R. Mittal, S. Balachandar. Direct numerical simulation of flow past elliptical cylinders Journal of Computational Physics 124, 351-367 (1996).

[7] http://www.featflow.de

[8] http://en.wikipedia.org/